Carbon 157 (2020) 113–119

Contents lists available at ScienceDirect

Carbon

journal homepage: www.elsevier.com/locate/carbon

Current density effect on current-carrying friction of amorphous carbon film

Kun Sun [a, b], Dongfeng Diao [a, *]

[a] Institute of Nanosurface Science and Engineering (INSE), Guangdong Provincial Key Laboratory of Micro/Nano Optomechatronics Engineering, Shenzhen University, Shenzhen, 518060, China
[b] Key Laboratory of Education Ministry for Modern Design and Rotor-Bearing System, Xi'an Jiaotong University, Xi'an, 710049, China

ARTICLE INFO

Article history:
Received 31 July 2019
Received in revised form
8 September 2019
Accepted 2 October 2019
Available online 3 October 2019

Keywords:
Current density
Graphene nanosheets
Amorphous carbon
Current-carrying friction

ABSTRACT

We report the current density effect in controlling current-carrying friction of amorphous carbon (a-C) film sliding against steel ball. The current density at the sliding interface was set to a constant value or cyclic variation value by adjusting the current intensity and the contact area for exploring the current-carrying friction behavior. The results showed that when the current density enhanced from 0 to 0.196 mA/μm^2, the friction coefficient decreased from 0.20 to 0.03 and the run-in cycle shortened from about 100 to few cycles. When the current density cyclically varied during the sliding, the friction coefficient had a very fast response and followed to the corresponding value which can be adjusted by the current density. Raman spectrum analysis and TEM observation confirmed that graphene nanosheets were formed at the sliding interface and the size of graphene nanosheets depended on the current density. The mechanism of current-carrying friction behavior of a-C film sliding against steel ball was the interactions of graphene to graphene and a-C to a-C at the contact area, which was controlled by the current density. This finding shed light on the great role of the current density in current-carrying friction of a-C film.

© 2019 Elsevier Ltd. All rights reserved.

1. Introduction

With a fast development of novel batteries [1–3], electric cars [4] and high-speed railways [5], people pay more attentions to the electrical contact elements and care their current-carrying friction behaviors. The electrical contact elements play an important role in controlling the moving parts and transmitting the electrical signals or electric powers [6–8]. Generally, the current-carrying friction between two electrical contact surfaces has a direct influence on the precision, reliability and durability of the whole electrical contact systems. In the past, most researches mainly focus on developing the electrical contact materials to improve the conductive and tribological properties [9–15]. Although a series of conductive materials are intensively studied, the high friction and the high wear still exists in the practical applications. Recently, some studies attempt to lubricate the electrical contact surfaces with thin-film materials, such as molybdenum disulfide, graphite and graphene. In the literatures, it is reported that the friction coefficients of the thin-film materials had some decrease under the current condition, which showed that the thin-film materials had a potential in reducing the friction of the electrical contact surfaces [16–19]. However, the mechanism of the decreased friction was not clear.

Amorphous carbon (a-C), as one impotent thin-film material, is a metastable structure composed of sp^2 and sp^3 bonds, which possesses excellent mechanical performances, low friction properties and variable electrical characteristics [20–24]. On one hand, the a-C film is an important solid-lubricating material with a big range of friction coefficient values, which is widely accepted in reducing the friction and wear of the metal surfaces and prolonging the lifetime of the metal products [25–30]. On other hand, the electrical characteristics of a-C film can be regulated with different proportions of sp^2 and sp^3 bonds, which may provide a good electron transport property for the carbon/metal interface [31,32]. From the viewpoints of tribology and electronics, the a-C film has a potential for reducing the friction between the electrical contact surfaces. In our recent work, we applied a high-intensity current at the a-C/steel sliding interface and obtained a low friction behavior [33]. However, the role of current intensity or current density on

* Corresponding author.
E-mail address: dfdiao@szu.edu.cn (D. Diao).

https://doi.org/10.1016/j.carbon.2019.10.005
0008-6223/© 2019 Elsevier Ltd. All rights reserved.

the friction behavior was not studied, and which was of the essence in controlling the friction behavior was still not clear.

In this study, we investigated the effect of current density on the current-carrying friction behavior of a-C film sliding against steel ball. The different current density was achieved by turning the current intensity and changing the contact area. The friction properties with the constant current density and the cyclic current density were studied. Raman spectrum analysis and TEM observation of transfer film were carried out to reveal the effect of current density on the friction behavior. And the mechanism for the current density effect on current-carrying friction of a-C film was discussed.

2. Experimental details

2.1. Current-carrying friction test of a-C film

Current-carrying friction tests of the a-C film/steel ball sliding interface were performed by a liner reciprocating ball-on-plate tribometer, which was schematically shown in Fig. 1. The detailed tests of friction force had been reported in our previous works [33]. The a-C film with thickness of 100 nm was fabricated on p-silicon <100> substrate (resistivity: < 0.0015 Ω cm) by a divergent electron cyclotron resonance (DECR) plasma sputtering system with the ion irradiation energy of 10 eV [34]. The steel ball materials were GCr15 (AISI 52100) bearing steel. The normal force was 3 N. The sliding velocity was 5.0 mm/s, and the stroke length was 20 mm. The currents with a constant value or cyclic values were applied at the a-C/steel sliding interface. The friction tests were operated in a clean room with the temperature of 25–27 °C and the relative humidity of 50–60%. Each test was repeated more than five times.

After the friction tests, the morphologies of transfer films were observed by an optical microscope (Nikon Eclipse LV150 N). The bonding structures of the original a-C film and the transfer films were analyzed by Raman spectra (Horiba, HR-Resolution) obtained with a laser wave length of 532 nm. The D band and G band were fitted with a Lorentzian line and a Breit-Fano-Wagner (BFW) line, respectively. The nanostructures of transfer films were observed by using a double spherical aberration corrected transmission electron microscope (TEM, Thermo Fisher, Titan3 Themis G2 300) with the electron accelerating voltage was 80 kV. The cross-sectional TEM specimens were cut from transfer film, and progressively thinned to about 100 nm by using a focused ion beam (FIB, Thermo Fisher, Scios).

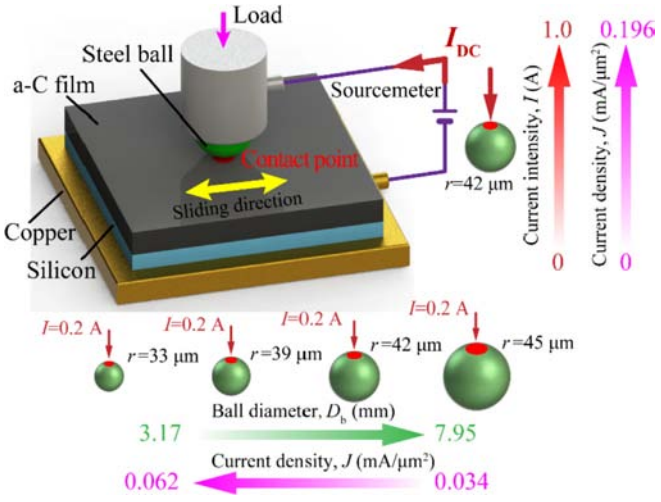

Fig. 1. Schematic diagram of friction test apparatus with different current densities for a-C film/steel ball sliding interface. The different current densities were achieved by tuning the current intensity from 0 to 1.0 A and changing the diameter of steel ball from 3.17 to 7.95 mm. (A colour version of this figure can be viewed online.)

2.2. Current density control method

The current density (J) at the a-C film/steel ball contact interface was calculated with Equation (1):

$$J = I/S = I/\pi r^2 \tag{1}$$

where I was the current intensity, S was the contact area, and r was the radius of the contact area. According to the Hertz contact theory [35], the radius of contact area (r) was calculated with Equation (2):

$$r = \left(\frac{3}{8} D_b F_N \left(\frac{1-\mu_s^2}{E_s} + \frac{1-\mu_b^2}{E_b}\right)\right)^{1/3} \tag{2}$$

where D_b was the diameter of steel ball, F_N was the normal load, μ_s and μ_b was the Poisson's ratio for silicon substrate and steel ball, E_s and E_b was the elastic modulus for silicon substrate and steel ball. In order to achieve different current densities, two methods were carried out and the detail was indicated in Fig. 1. For the first method, the current density was controlled by tuning the applied current intensity. The current intensity was adjusted with a range from 0 to 1.0 A and the steel ball was kept with one constant diameter of 6.35 mm, then the current density varied from 0 to 0.196 mA/μm^2. For the second method, the current density was controlled by adjusting the contact area. The current intensity was set as a constant value (0.2 A) and the steel balls with the diameters of 3.17, 3.96, 4.78, 5.56, 6.35, 7.14 and 7.95 mm were selected to obtain the different contact areas. Then the current density was controlled from 0.034 to 0.062 mA/μm^2.

3. Results and discussions

3.1. Current density effect on current-carrying friction behavior of a-C film

Fig. 2 shows the effect of constant current density on the friction behavior of a-C film/steel ball sliding interface. Fig. 2(a) shows the friction curves of a-C film sliding against steel ball with the diameter of 6.35 mm under different current intensities. It was observed that as the current intensity enhanced from 0 to 1.0 A, the run-in cycle shortened from 120 to few cycles and the friction coefficient at 150 cycles position (stable stage) decreased from 0.20 to 0.03. The details are that when the current intensity was less than 0.3 A, the friction coefficient started with 0.16–0.18 and increased, then after several dozens of cycles (run-in stage), the friction coefficient decreased and maintained thereafter. When the current intensity was more than 0.4 A, the friction coefficient started with 0.16–0.18 and rapidly decreased to 0.03–0.05 with a few cycles (run-in stage), and maintained thereafter. Fig. 2(b) exhibits the friction curves of a-C film sliding against the steel balls with different diameters under 0.2 A current intensity. It could be observed that as the diameter of steel balls decreased from 7.94 to 3.28 mm, the run-in cycle shortened from 60 to 25 cycles and the friction coefficient at 150 cycles position (stable stage) decreased from 0.10 to 0.04. The details are that the friction coefficient started with 0.16–0.18 and increased, then after a few dozens of cycles (run-in stage), the friction coefficient quickly decreased and maintained thereafter.

Based on the data showing in Fig. 2, the relationship between current density and friction behavior was summarized in Fig. 3. Fig. 3(a) shows the relationship between the current density and

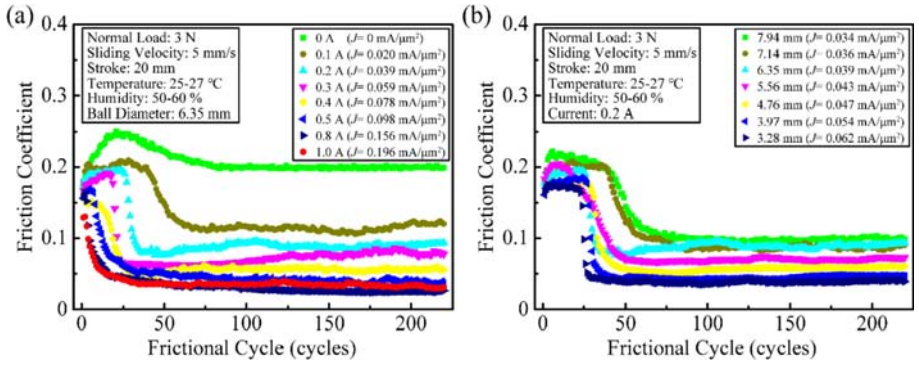

Fig. 2. The effect of constant current density on the friction behavior of a-C film/steel ball sliding interface. (a) Friction curves of a-C film sliding against steel ball with the diameter of 6.35 mm under the 0–1.0 A current intensities, (b) Friction curves of a-C film sliding against steel ball with the diameter varied from 3.28 to 7.94 mm under 0.2 A constant current intensity. (A colour version of this figure can be viewed online.)

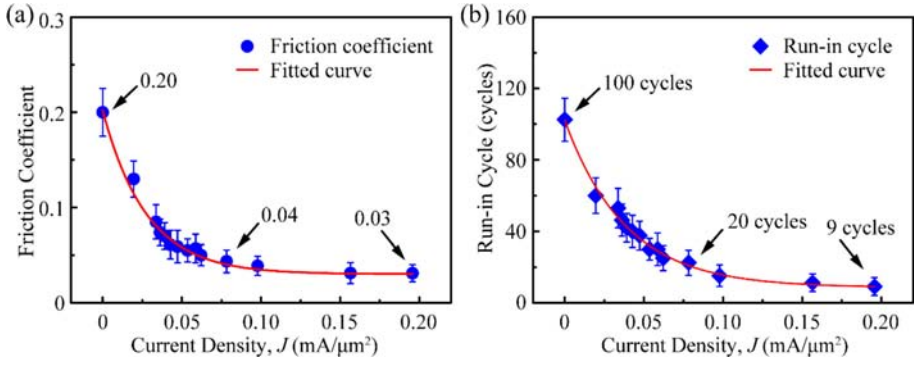

Fig. 3. Current density effect on friction behavior. (a) The relationship between current density and friction coefficient, (b) The relationship between current density and run-in cycle. (A colour version of this figure can be viewed online.)

the friction coefficient at 150 cycles position, which was in the stable stage. It could be seen that when the current density enhanced from 0 to 0.08 mA/μm^2, the friction coefficient sharply decreased from 0.20 to 0.04, and as the current density further enhanced over 0.08 mA/μm^2, the friction coefficient had no obvious change and kept at 0.03. Fig. 3(b) shows the relationship between the current density and the run-in cycle. It could be found that as the current density enhanced from 0 to 0.08 mA/μm^2, the run-in cycle decreased from 100 to 20 cycles, and as the current density was over 0.08 mA/μm^2, the run-in cycle had no obvious change. Based on the above analyses, it could be concluded that the current density directly influenced on the friction behavior of a-C film.

Fig. 4 shows the effect of cyclic current density on the friction behavior of a-C film/steel ball sliding interface. Fig. 4(a) shows the friction curve of a-C film sliding against steel ball with intermittently applying the current of 1.0 A. During the sliding, once the current turned on, the friction coefficient immediately decreased from 0.20 to 0.05 with 1 cycle, and as the current turned off, the friction coefficient also quickly returned to 0.20 with ~2 cycles. It was indicating that the friction coefficient had a fast response to the current. Fig. 4(b) shows the friction curve of a-C film sliding against steel ball with alternately applying different currents with 1.0 A, 0.5 A, 0.3 A, and 0.1 A. It could be observed that during the sliding, as the different currents was alternately applied, the friction coefficient fast responded and changed to the corresponding values, and as the currents turned off, the friction coefficient quickly returned to 0.20. It was meaning that the friction coefficient of a-C film can be real-time controlled. Fig. 4(c) shows the friction curve of a-C film sliding against steel ball with two cycle monotonically increasing the current from 0 to 0.5 A. It was clear found that the friction coefficient was monotonically controlled from 0.20 to 0.05. Furthermore, as the current randomly applied during the sliding, the friction coefficient also had a fast response and changed to the corresponding values, as shown in Fig. 4(d). Based on the above analyses, it was further confirmed that the current density had a direct effect on the friction behavior of a-C film. Besides, the controlling friction behavior of a-C film with the cyclic current density showed a big potential in the real-time friction control.

3.2. Characterizations of transfer films

Fig. 5 shows the morphologies and Raman spectrum of transfer films with different current densities. Fig. 5(a) shows the optical images of worn surfaces on steel ball with the diameter of 6.35 mm under different current intensities. For no current condition, little carbon materials were observed on the steel surface. Some transfer fragments were covered on the middle of worn surface, and more wear debris were accumulated at the two sides along the sliding direction. While for current-carrying conditions, more carbon materials were covered on the middle of worn surface with forming a thick transfer film, and the carbon transfer film became much thicker and flatter with the current intensity enhanced. Fig. 5(b) shows that the Raman spectra of transfer film with different current intensities, and the test points were marked in the optical images. For no current condition, the Raman spectrum showed a weak signal with no obvious carbon signals (G band or D band), meaning that the transfer film was not thick enough. While for current-

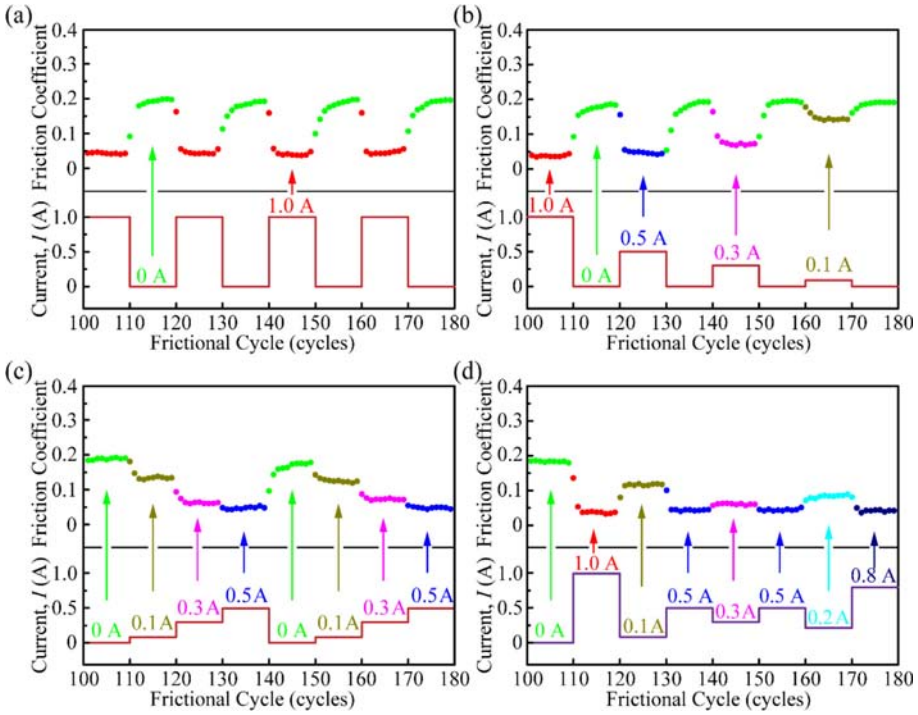

Fig. 4. The effect of cyclic current density on the friction behavior of a-C film/steel ball sliding interface. (a) Friction curve of a-C film sliding against steel ball with intermittently applying the current of 1.0 A. (b) Friction curve of a-C film sliding against steel ball with alternately applying different current with 1.0 A, 0.5 A, 0.3 A and 0.1 A. (c) Friction curve of a-C film sliding against steel ball with monotonically enhancing the current from 0 to 0.5 A. (d) Friction curve of a-C film sliding against steel ball with randomly applying the different currents. (A colour version of this figure can be viewed online.)

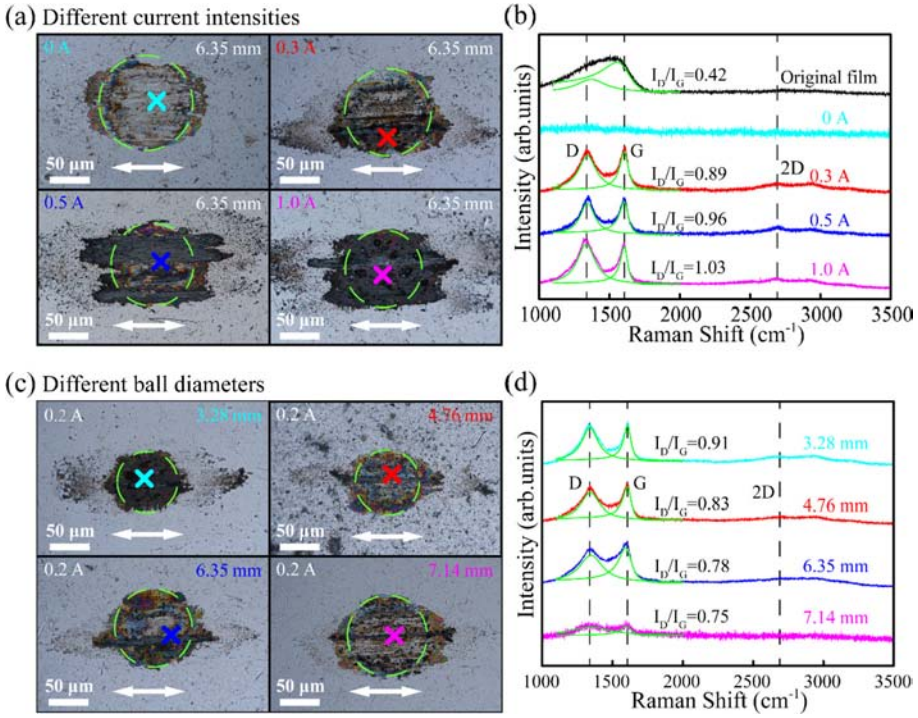

Fig. 5. The morphologies and Raman spectrum analyses of transfer films with different current densities. (a) Optical images and (b) Raman spectra of transfer films on steel ball with the diameter of 6.35 mm under different current intensities, (c) Optical images and (d) Raman spectra of transfer films on the steel ball with different diameters under 0.2 A current intensity. (A colour version of this figure can be viewed online.)

carrying conditions, the Raman spectra contained the separated D and G bands around 1350 cm^{-1} and 1580 cm^{-1}. Compared with the original a-C film, the independent D band and G band indicated that some carbon nanocrystallites existed in the transfer film. And the ratio of D band to G band (I_D/I_G) increased with the current intensity enhanced. Fig. 5(c) shows the optical images of worn surfaces on steel ball with different diameters under 0.2 A current-carrying condition. For the small ball, a thick transfer film was covered on the steel surface. As the diameter of steel ball increased, the transfer film became incomplete. As for the large ball, the transfer film was very thin, which was closed to the transfer film without current. Fig. 5(d) shows that the Raman spectra of transfer film on the steel ball with different diameters. The independent D band and G band indicated that the transfer film contained carbon nanocrystallites. And the I_D/I_G value decreased with the ball diameter increased. Based on the above analyses, it could be confirmed that as the current density enhanced, the transfer film became thicker and flatter, meanwhile, their I_D/I_G value increased.

The detailed relationship between the current density and the I_D/I_G value was summarized in Fig. 6(a). When the current density was less than 0.04 mA/μm^2, the I_D/I_G value was difficult to be calculated with the weak signal of Raman spectra (similar to 0 A case in Fig. 5(b)). When the current density was at the range from 0.04 to 0.08 mA/μm^2, the I_D/I_G value increased with the current density enhanced. And when the current density was more than 0.08 mA/μm^2, the I_D/I_G value had no obvious change. Based on the I_D/I_G value, the in-plane size (L_α) of carbon nanocrystallites in transfer film was estimated with $I_D/I_G = C(\lambda)\ L_\alpha^2$, where $C(\lambda)$ is 0.55 nm^{-2}, related to excitation laser wavelength [36]. Fig. 6(b) shows the relationship between the current density and the size of carbon nanocrystallites. When the current density was less than 0.04 mA/μm^2, the L_α of carbon nanocrystallites could not be calculated with the weak signal of Raman spectra. When the current density was at the range from 0.04 to 0.08 mA/μm^2, the L_α had an increase from 1.19 nm to 1.30 nm with the current density enhanced. When the current density was more than 0.08 mA/μm^2, the L_α had no obvious increase and kept at 1.33 nm. Although the values of I_D/I_G and L_α could not be obtained with low current density because of the weak signal of Raman spectra, it still could be concluded that the size of carbon nanocrystallites in transfer film increased with the current density enhanced.

Fig. 7 shows the TEM images of transfer films with different current densities. For no current condition, Fig. 7(a) shows the low-resolution TEM images of the transfer film at the 2400 cycles position (this is over the 240 cycles showing in Fig. 2(a) to obtain a thick enough transfer film for TEM observation). It could be found that the thickness of transfer film was about 100 nm. While for current-carrying conditions, the transfer films became much thicker. From the low-resolution TEM images (Fig. 7(b)–(d)), the thickness of transfer film at the 240 cycles position was about 160 nm, 240 nm and 350 nm for the current density of 0.039 mA/μm^2, 0.098 mA/μm^2 and 0.196 mA/μm^2, respectively. The nanostructures of transfer film were further observed from the high-resolution TEM images. For no current condition, Fig. 7(e) shows that the transfer film was close to amorphous structure, and the faster Fourier transformed filtering of the selected area 1 (FFT_1) with a dim diffuse ring also indicated that the structure was amorphous-like. For the current-carrying conditions, the transfer films were a coupling structure of graphene nanosheets embedded in amorphous matrix. Fig. 7(f)–(h) show that the stacks of graphene layers were distributed in amorphous structure, and the orientations were approximately parallel to the steel surface, which coincided with the sliding direction. The faster Fourier transformed filtering of the selected area 2, 3 and 4 all showed a pair of light shots, indicating that the existence of graphene nanosheets in the transfer films. Further comparing the structures of transfer film under different current-carrying conditions, for the low current density of 0.039 mA/μm^2, the transfer film contained small-sized graphene nanosheets (Fig. 7(f)), while for the high current density of 0.098 mA/μm^2, the transfer film owned the enlarged graphene nanosheets (Fig. 7(g)), and for the further high current density of 0.196 mA/μm^2, the size of graphene nanosheets did not increase obviously (Fig. 7(h)). The TEM analyses on the size of graphene nanosheets were in accord with the Raman analyses. Combining the TEM and Raman analyses, it could be concluded that the size of graphene nanosheets in transfer film depended on the current density.

3.3. *Mechanism for current density effect on current-carrying friction*

Based on the above analyses of friction behaviors and characterizations of transfer films, the mechanism for the current density effect on current-carrying friction behavior of a-C film/steel ball sliding interface was summarized in Fig. 8. For no current (zero current density) condition, a few a-C fragments from the original a-C film transferred to the steel ball and formed a very thin a-C transfer film, then the whole a-C/a-C interaction at the sliding interface led to a high friction, as shown in Fig. 8(a). As the current flowed through the a-C/steel contact interface, the graphene

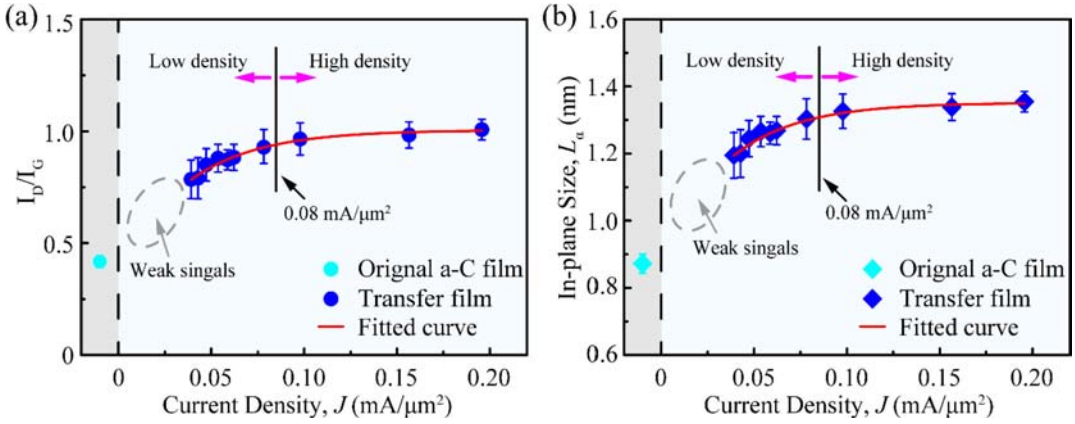

Fig. 6. Current density effect on the I_D/I_G and the L_α of transfer film. (a) The relationship between the current density and the I_D/I_G, (b) the relationship between the current density and the in-plane size. (A colour version of this figure can be viewed online.)

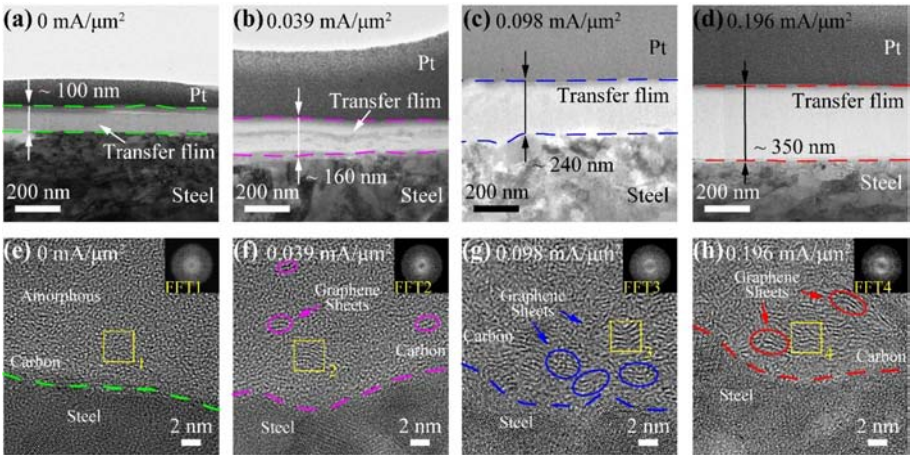

Fig. 7. The cross-sectional nanostructures of the transfer films on steel balls. a)-d) Low-resolution TEM images, e)-h) High-resolution TEM images of transfer film with different current densities. Inset figures in e)-h) show FFT images of the selected area in high resolution TEM images. (A colour version of this figure can be viewed online.)

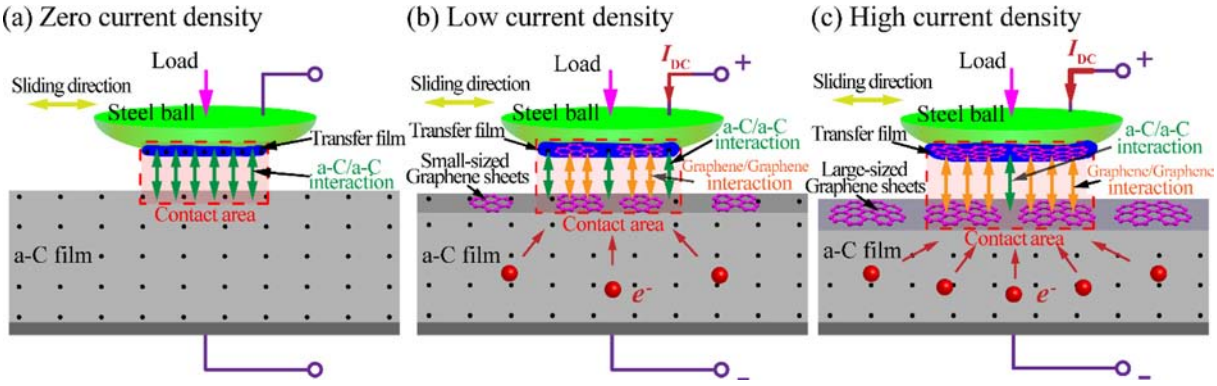

Fig. 8. The friction mechanism with different current densities. (a) For zero current density, the sliding interface was amorphous carbon, and the whole a-C/a-C interaction led to a high friction. (b) For low current density, small-sized graphene nanosheets formed at the sliding interface, and a small proportion of graphene/graphene interaction led to a reduced-friction. (c) For high current density, large-sized graphene nanosheets formed at the sliding interface, and a large proportion of graphene/graphene interaction led to a low friction. (A colour version of this figure can be viewed online.)

nanosheet was formed at the top-surface of a-C film, which was easily wore out and transferred to the counter surface. Then, a thick transfer film with a coupling structure of graphene nanosheets embedded in amorphous carbon was formed on the steel ball. The graphene/graphene interaction at the sliding interface provided the weak shear force for reducing the friction. For the low current density, Fig. 8(b) shows that a little number of electrons flowed through the contact area, and the small-sized graphene nanosheets was formed at the sliding interface (as confirmed in Fig. 7(f)), which led to a low proportion of graphene/graphene interaction between the two sliding surfaces. Then the low proportion of graphene/graphene interaction led to a reduced friction. For the high current density, Fig. 8(c) shows that large amounts of electrons flowed through the contact area, and the large-sized graphene nanosheets was formed at the sliding interface (as confirmed in Fig. 7(g) and (h)), which largely increased the proportion of graphene/graphene interaction. The high proportion of graphene/graphene interaction led to a low friction. Furthermore, if the graphene/graphene interaction was distributed at the whole sliding interface, the friction coefficient was believed to further reduce at the ultra-low friction level.

As for the mechanism on the cyclic current density controlling the friction of a-C film/steel ball sliding interface, it was mainly due to the alternation of graphene nanosheets in transfer film. During the sliding process, as the current density was varied with different values, the previous formed graphene nanosheets was easy to be worn out and the new formed graphene nanosheets were determined by the varied current density, which could adjust the proportion of graphene/graphene and a-C/a-C interactions at the sliding interface, then control the friction coefficient.

Thus, it was concluded that the current-carrying friction behavior of a-C film can be controlled with the proportion of graphene to graphene and a-C to a-C interactions at the sliding interface, which strongly depended on the current density. This finding might be expected for controlling the friction coefficients of a-C film in many tribo-industrial applications.

4. Conclusions

In summary, the current-carrying friction behavior and mechanism of amorphous carbon film sliding against steel ball were studied. The effect of the current density in controlling current-carrying friction was clarified. The friction coefficient and run-in cycle of current-carrying friction were controlled by the interactions of graphene to graphene and a-C to a-C at the contact area, which strongly depended on the current density. The detail conclusions were given by the following. (1) For the constant current density effect, as the current density increased from 0 to

0.196 mA/μm^2, the friction coefficient decreased from 0.20 to 0.03 and the run-in cycle decreased from 100 to few cycles. (2) For the cyclic current density effect, as the current density varied cyclically during the sliding, the friction coefficient had a fast response and changed to the corresponding value. (3) The current-carrying friction behavior was controlled by the size of graphene nanosheets at the sliding interface, which was controlled by the current density. This finding shed light on the great role of the current density in current-carrying friction of a-C film and developed the its application in protecting the electrical contact surfaces.

Acknowledgements

The authors would like to thank the financial support of National Natural Science Foundation of China (No. 51975383), Shenzhen Fundamental Research and Discipline Layout Project (JCYJ20160427105015701). The authors would like to the Electron Microscope Center (EMC) of Shenzhen University for the help in TEM observations with double spherical aberration corrected transmission electron microscope.

References

[1] G.J. May, A. Davidson, B. Monahov, Lead batteries for utility energy storage: a review, J. Energy Storage 15 (2018) 145–157.
[2] X. Luo, J. Wang, M. Dooner, J. Clarke, Overview of current development in electrical energy storage technologies and the application potential in power system operation, Appl. Energy 137 (2015) 511–536.
[3] S.A. Pervez, M.A. Cambaz, V. Thangadurai, M. Fichtner, Interface in solid-state Li battery: challenges, progress and outlook, ACS Appl. Mater. Interfaces 11 (2019) 22029–22050.
[4] J. Tollefson, Car industry: charging up the future, Nature 456 (2008) 436–440.
[5] R. He, B. Ai, G. Wang, K. Guan, Z. Zhong, A.F. Molisch, et al., High-speed railway communications: from GSM-R to LTE-R, IEEE Veh. Technol. Mag. 11 (2016) 49–58.
[6] R. Holm, Electric Contacts: Theory and Application, Springer, Berlin, 2013.
[7] F. Léonard, A.A. Talin, Electrical contacts to one- and two-dimensional nanomaterials, Nat. Nanotechnol. 6 (2011) 773–783.
[8] M. Kalin, D. Poljanec, Influence of the contact parameters and several graphite materials on the tribological behaviour of graphite/copper two-disc electrical contacts, Tribol. Int. 126 (2018) 192–205.
[9] M. Grandin, U. Wiklund, Friction, wear and tribofilm formation on electrical contact materials in reciprocating sliding against silver-graphite, Wear 302 (2013) 1481–1491.
[10] A. Bouchoucha, S. Chekroud, D. Paulmier, Influence of the electrical sliding speed on friction and wear processes in an electrical contact copper-stainless steel, Appl. Surf. Sci. 223 (2004) 330–342.
[11] H. Jiang, Y. Meng, S. Wen, H. Ji, Effects of external electric fields on frictional behaviors of three kinds of ceramic/metal rubbing couples, Tribol. Int. 32 (1999) 161–166.
[12] N. Argibay, W.G. Sawyer, Low wear metal sliding electrical contacts at high current density, Wear 274–275 (2012) 229–237.
[13] C. Deng, J. Yin, H. Zhang, X. Xiong, P. Wang, M. Sun, The tribological properties of Cf/Cu/C composites under applied electric current, Tribol. Int. 116 (2017) 84–94.
[14] D. Poljanec, M. Kalin, Effect of polarity and various contact pairing combinations of electrographite, polymer-bonded graphite and copper on the performance of sliding electrical contacts, Wear 426–427 (2019) 1163–1175.
[15] H. Lang, Y. Peng, G. Shao, K. Zou, G. Tao, Dual control of the nanofriction of graphene, J. Mater. Chem. C 7 (2019) 6041–6051.
[16] P. Wang, W. Yue, Z. Lu, G. Zhang, L. Zhu, Friction and wear properties of MoS_2-based coatings sliding against Cu and Al under electric current, Tribol. Int. 127 (2018) 379–388.
[17] Y. Zeng, F. He, Q. Wang, X. Yan, G. Xie, Friction and wear behaviors of molybdenum disulfide nanosheets under normal electric field, Appl. Surf. Sci. 455 (2018) 527–532.
[18] J.A. Bares, N. Argibay, P.L. Dickrell, G.R. Bourne, D.L. Burris, J.C. Ziegert, et al., In situ graphite lubrication of metallic sliding electrical contacts, Wear 267 (2009) 1462–1469.
[19] D. Berman, A. Erdemir, A.V. Sumant, Graphene as a protective coating and superior lubricant for electrical contacts, Appl. Phys. Lett. 105 (2014) 231907.
[20] J. Robertson, Diamond-like amorphous carbon, Mater. Sci. Eng. R 37 (4) (2002) 129–281.
[21] S. Hirono, S. Umemura, M. Tomita, R. Kaneko, Superhard conductive carbon nanocrystallite films, Appl. Phys. Lett. 80 (2002) 425–427.
[22] P. Manimunda, A. Al-Azizi, S.H. Kim, R.R. Chromik, Shear-induced structural changes and origin of ultralow friction of hydrogenated diamond-like carbon (DLC) in dry environment, ACS Appl. Mater. Interfaces 9 (2017) 16704–16714.
[23] K. Lee, H. Ki, Rapid fabrication of transparent conductive films with controllable sheet resistance on glass substrates by laser annealing of diamond-like carbon films, Acta Mater. 111 (2016) 315–320.
[24] K. Sun, D. Diao, L. Yang, W. Zhang, X. Fan, Nanosized graphene sheets enhanced electron field emission behavior in pure carbon film, Thin Solid Films 664 (2018) 124–129.
[25] C. Donnet, A. Erdemir, Tribology of Diamond-like Carbon Films: Applications and Future Trends in DLC's Tribology, Springer, New York, 2007, p. 457.
[26] Y. Wang, K. Gao, B. Zhang, Q. Wang, J. Zhang, Structure effects of sp^2-rich carbon films under super-low friction contact, Carbon 137 (2018) 49–56.
[27] N. Dwivedi, R.J. Yeo, Z. Zhang, C. Dhand, S. Tripathy, C.S. Bhatia, Interface engineering and controlling the friction and wear of ultrathin carbon films: high sp^3 versus high sp^2 carbons, Adv. Funct. Mater. 26 (2016) 1526–1542.
[28] S. Bhowmick, M.Z.U. Khan, A. Banerji, M.J. Lukitsch, A.T. Alpas, Low friction and wear behaviour of non-hydrogenated DLC (a-C) sliding against fluorinated tetrahedral amorphous carbon (ta-CF) at elevated temperatures, Appl. Surf. Sci. 450 (2018) 274–283.
[29] B. Bhushan, X. Li, Micromechanical and tribological characterization of hard amorphous carbon coatings as thin as 5 nm for magnetic recording heads, Wear 220 (1) (1998) 51–58.
[30] A. Erdemir, C. Donnet, Tribology of diamond-like carbon films: recent progress and future prospects, J. Phys. D Appl. Phys. 39 (2006) R311–R327.
[31] P. Xue, C. Chen, D.F. Diao, Ultraesensitive flexible strain sensor based on graphene nanocrystallite carbon film with wrinkle structure, Carbon 147 (2019) 227–235.
[32] E.H.T. Teo, A. Bolker, R. Kalish, C. Saguy, Nano-patterning of through-film conductivity in anisotropic amorphous carbon induced using conductive atomic force microscopy, Carbon 49 (2011) 2679–2682.
[33] K. Sun, X. Fan, W. Zhang, P. Xue, D. Diao, Contact-focusing electron flow induced nanosized graphene sheets formation in amorphous carbon film for fast low-friction, Carbon 149 (2019) 45–54.
[34] C. Chen, P. Xue, X. Fan, C. Wang, D.F. Diao, Friction-induced rapid restructuring of graphene nanocrystallite cap layer at sliding surfaces: short run-in period, Carbon 130 (2018) 215–221.
[35] K.L. Johnson, Contact Mechanics, Cambridge University Press, New York, 1987, p. 90.
[36] A.C. Ferrari, J. Robertson, Interpretation of Raman spectra of disordered and amorphous carbon, Phys. Rev. B 61 (2000) 14095–14106.